Vibronic structure of the emission spectra from single vibronic levels of the S 1 manifold in naphthalene: Theoretical simulation

Fabrizia Negri and Marek Z. Zgierski

Citation: The Journal of Chemical Physics **104**, 3486 (1996); doi: 10.1063/1.471054
View online: http://dx.doi.org/10.1063/1.471054
View Table of Contents: http://scitation.aip.org/content/aip/journal/jcp/104/10?ver=pdfcov
Published by the AIP Publishing

Vibronic structure of the emission spectra from single vibronic levels of the S_1 manifold in naphthalene: Theoretical simulation

Fabrizia Negri
Dipartimento di Chimica "G. Ciamician," Università di Bologna, 40126 Bologna, Italy

Marek Z. Zgierski
Steacie Institute for Molecular Sciences, National Research Council of Canada, Ottawa, K1A 0R6 Canada

(Received 16 June 1995; accepted 27 September 1995)

The vibrational structure of electronic spectra of naphthalene is simulated by means of a perturbative calculation of the intensities, based on the vibronic basis set. The formalism is implemented to include the contribution of Herzberg–Teller induced activity for totally symmetric modes and to describe the interference between the latter and the allowed Franck–Condon intensity. Geometries, vibrational normal modes, and vibronic coupling parameters required to model the spectra are obtained by means of *ab initio* and semiempirical calculations. The structure of absorption and single vibronic level fluorescence spectra is reproduced in detail and consistently for all the spectra examined. It is shown that the intensity of modes ν_{8a} and ν_{5a} is strongly affected by interference effects, and that Dushinsky mode mixing of totally symmetric modes plays a major role in redistributing the intensity among the vibronic bands of the spectra. © *1996 American Institute of Physics.* [S0021-9606(96)02309-3]

I. INTRODUCTION

Vibronic structure of the $S_0 \rightarrow S_1$ electronic transitions in naphthalene belongs to more interesting cases occurring in aromatic hydrocarbons. The four lowest excited states of these molecules correspond, according to the perimeter model,[1–3] to the promotion of an electron from the highest occupied molecular orbital (HOMO) to the lowest unoccupied molecular orbital (LUMO). Both these orbitals are doubly degenerate in this model, and as a result, the lower L_a and L_b states do not couple with the ground state via electric dipole moment, while the higher, degenerate B state is strongly coupled to the ground state by this interaction. This is the situation in benzene where the L_a state becomes $B_{1u}(S_2)$, the L_b state becomes $B_{2u}(S_1)$ and the B state becomes E_{1u}. When crosslinks are introduced between carbon atoms, the degeneracies of the HOMO and LUMO are lifted. In consequence, the $S_0 \rightarrow L$ transitions become weakly allowed, that to the L_b state being much less intense than the transition to L_a state, while the B state splits into B_a and B_b components. The energy ordering of the L_a and L_b states in naphthalene is the same as in benzene (L_b being the lowest excited singlet), however, the gap between the L states becomes much smaller. In anthracene, the ordering becomes inverted, and, as a result, the L_b state is hidden in the absorption under much more intense transition to the L_a state. The very small oscillator strength of the $S_0 \rightarrow S_1$ transition in naphthalene makes vibronic interactions with higher electronic states a very important source of intensity for this transition. The interactions of the $L_b(1B_{2u})$ state with the $B_b(2B_{2u})$ state occur via totally symmetric (TS) a_g modes, and with the $L_a(1B_{1u})$ and the $B_a(2B_{1u})$ states occur via nontotally symmetric (NTS) b_{3g} modes. Thus the $S_0 \rightarrow S_1$ transition is a prime example of manifestation of both Franck–Condon and vibronic effects in the absorption and emission spectra of a large polyatomic molecule. It is also an interesting example of the interference between Franck–Condon (FC) and Herzberg–Teller (HT) mechanism and its effect on intensities of individual vibronic lines.

The experimental ground state vibrational frequencies of naphthalene in solid and gas phases as well as for solution have been reported and discussed on the basis of scaled quantum mechanical (SQM) force field by Sellers *et al.*[4] Well resolved single vibronic level (SVL) emission spectra from individual vibronic levels of the S_1 manifold of naphthalene were studied in the gas phase by Stockburger, Gatterman and Klusman (SGK).[5] Some aspects connected with the intensities of lines associated with the $\nu_{8a}(a_g)$ and $\nu_{8b}(b_{3g})$ modes were subsequently studied by us in a model fashion.[6] The S_1 state frequencies of the in-plane modes were discussed in a number of papers.[7–9] Fluorescence excitation spectra of naphthalene in a supersonic jet have been subsequently reported by Beck *et al.*[10] They provided the well resolved absorption spectrum up to 6000 cm^{-1} above the origin of the $S_0 \rightarrow S_1$ transition. Compared with the 0_0^0 level emission they show strong breakdown of the mirror symmetry between absorption and emission which is not surprising for a weak transition where most of the intensity is vibronically induced. Single vibronic level emission spectra in a supersonic jet were then reported by Beck *et al.*[11] and by Behlen *et al.*[12] They complement the spectra of SGK giving emission from new vibronic levels, in particular the $(\nu_{4a})_0^1$ level of S_1.

We have demonstrated by model simulations[6] that nonadiabatic and non-Condon effects have to be taken into account if one wants to understand distributions of vibronic intensities in SVL emission spectra. The simulation of these spectra requires input parameters which can be obtained from quantum-chemical calculations. These are displacement parameters describing geometry differences between elec-

 0021-9606/96/104(10)/3486/15/$10.00

TABLE I. The calculated bond lengths (in Å) and bond angles (in deg) of the carbon skeleton of naphthalene in the S_0, S_1, and S_2 states.

Parameter[a]	Expt.	QCFF/PI+CIS	QCFF/PI+CISD	CIS/6-31G*	CIS/6-31+G	CASSCF/DZV[b]
			$S_0(1A_g)$			
C_1C_2	1.425[c]	1.4367	1.4368	1.4205		1.433
C_1C_6	1.424	1.4407	1.4424	1.4092		1.422
C_2C_3	1.377	1.3856	1.3882	1.3583		1.383
C_3C_4	1.417	1.4247	1.4267	1.4166		1.430
$C_6C_1C_2$		119.14	119.16	118.97		
$C_1C_2C_3$		120.21	120.18	120.78		
$C_2C_3C_4$		120.65	120.66	120.25		
			$S_1(1B_{2u})$			
C_1C_2	1.425[d]	1.4305	1.4243	1.4031	1.4062	1.420
C_1C_6	1.478	1.4897	1.5018	1.4911	1.4908	1.509
C_2C_3	1.422	1.4060	1.4124	1.3910	1.3944	1.422
C_3C_4	1.417	1.4331	1.4327	1.4103	1.4137	1.434
$C_6C_1C_2$		118.93	118.89	118.19	118.24	
$C_1C_2C_3$		120.26	120.33	121.43	121.48	
$C_2C_3C_4$		120.81	120.78	120.37	120.29	
			$S_2(1B_{1u})$			
C_1C_2			1.4230	1.4013		
C_1C_6			1.4648	1.4493		
C_2C_3			1.4392	1.4170		
C_3C_4			1.3892	1.3710		
$C_6C_1C_2$			119.16	118.41		
$C_1C_2C_3$			120.30	121.71		
$C_2C_3C_4$			120.54	119.88		

[a]Carbon atoms are numbered clockwise, C_1 and C_6 atoms belong to both aromatic rings.
[b]Reference 19.
[c]Reference 31.
[d]Reference 32.

tronic states coupled either by electric dipole or vibronically, vibronic coupling parameters and mode mixing matrices which map normal modes of one state onto those of another state. Robey *et al.*[13] were the first to present semiempirical (CNDO/S) calculations of vibronically induced transition dipole moments for the $S_0 \rightarrow S_1$ transition by the a_g and b_{3g} modes. No attempt to understand detailed vibronic structure of various SVL spectra was undertaken however in that paper. The present paper closes the gap between those two papers by bringing quantum-chemical calculations and modeling together to reproduce detailed vibronic structure of the observed absorption and SVL emission spectra of naphthalene. To this end we use semiempirical [QCFF/PI (Refs. 14, 15) and CNDO/S (Ref. 16)] and *ab initio*[17] methods to calculate all parameters needed for simulation of the spectra and the perturbation theory based on vibronic basis set[18] to calculate intensities of individual vibronic transitions.

In Sec. II we discuss the results of the quantum-chemical calculations in which parameters pertinent for the simulation of SVL spectra are obtained. Section III presents the general perturbation scheme adopted to simulate the intensities of individual vibronic transitions based on the vibronic basis set of wave functions.[18] Section IV reports the results of the simulations and discussion.

TABLE II. Vertical excitation energies (eV) of the electronic valence singlet states of naphthalene evaluated at the corresponding optimized S_0 state geometries and computed oscillator strengths of the $S_0 \rightarrow S_n$ transitions.

State	QCFF/PI+CIS	QCFF/PI+CISD	CNDO/S+CIS	CIS/6-31G*	CIS/6-31+G
S_1, $1B_{2u}$	4.11[a] (0.0032)[b]	3.88 (0.0032)	4.07 (0.0009)	5.54 (0.0003)	5.55 (0.0001)
S_2, $1B_{1u}$	4.47 (0.2408)	4.81 (0.1645)	4.28 (0.0690)	5.43 (0.0738)	5.44 (0.0925)
S_3, $2A_g$	5.35 (0.0000)	5.67 (0.0000)	5.68 (0.0000)	7.67 (0.0000)	7.41 (0.0000)
S_4, $1B_{3g}$	5.56 (0.0000)	5.72 (0.0000)	5.41 (0.0000)	7.27 (0.0000)	6.67 (0.0000)
S_5, $2B_{2u}$	5.84 (1.4113)	5.62 (1.9868)	6.07 (2.1959)	7.47 (2.3652)	7.16 (2.1411)
S_6, $2B_{1u}$	5.96 (0.7343)	6.23 (0.4320)	6.18 (0.8480)	7.63 (0.6896)	7.50 (0.7838)

[a]Excitation energy.
[b]Oscillator strength.

TABLE III. Vibrational frequencies (in cm^{-1}) of the in-plane normal modes (excluding CH stretches) in the $S_0(1A_g)$ state of naphthalene. Displacement parameters of the a_g modes for the $S_1 \rightarrow S_0$ and $S_2 \rightarrow S_0$ transitions are also listed. Calculated HF frequencies are scaled by 0.9.

	a_g			b_{3g}			b_{1u}			b_{2u}		
	QCCF/PI +CISD	HF/6-31G*	Expt.[a]	QCFF/PI	HF	Expt.[a]	QCFF	HF	Expt.[a]	QCFF	HF	Expt.[a]
ν_{3a}	1590 (0.19)[b] [0.65][c]	1605 (0.08)[d] [0.92][e] (0.01)[f]	1578	ν_{3b} 1633	1660	1624	1573	1625	1595	1507	1515	1509
ν_{4a}	1467 (0.16) [0.02]	1463 (0.22) [0.24] (0.28)	1460	ν_{4b} 1481	1461	1445	1412	1389	1389	1329	1328	1361
ν_{5a}	1336 (0.89) [1.44]	1338 (1.44) [1.74] (1.46)	1380	ν_{5b} 1296	1235	1240	1324	1251	1265	1169	1180	1209
ν_{6a}	1156 (0.12) [0.11]	1158 (0.01) [0.48] (0.05)	1163	ν_{6b} 1125	1146	1145	1135	1121	1125	1147	1074	1144
ν_{7a}	1005 (0.35) [0.11]	1035 (0.21) [0.01] (0.33)	1020	ν_{7b} 991	920	939	827	773	810	1030	968	1008
ν_{8a}	802 (0.72) [0.14]	748 (0.79) [0.09] (0.91)	761	ν_{8b} 548	499	508	413	350	359	699	607	619
ν_{9a}	516 (0.04) [0.56]	496 (0.24) [0.89] (0.42)	514									

[a]Reference 4.
[b]QCFF/PI+CISD $S_1 \rightarrow S_0$ displacement parameter.
[c]QCFF/PI+CISD $S_2 \rightarrow S_0$ displacement parameter.
[d]HF/6-31G*-CIS/6-31G* $S_1 \rightarrow S_0$ displacement parameter.
[e]HF/6-31G*-CIS/6-31G* $S_2 \rightarrow S_0$ displacement parameter.
[f]HF/6-31G*-CIS/6-31+G $S_1 \rightarrow S_0$ displacement parameter.

II. QUANTUM-CHEMICAL CALCULATIONS

The first *ab initio* study of the vibrational force field of the S_1 state of naphthalene molecule has been reported by Swiderek *et al.*[19] Multiconfiguration self-consistent field (MCSCF) method which includes all π-orbitals in its complete active space (CAS) formulation, was used with minimal and double-zed basis sets (STO-3G and DZV). The obtained force-field was then scaled according to the Pulay's procedure[20] in the same way as the corresponding force field of the ground electronic state. In the present paper, we use HF/6-31G* method for the ground state force field calculation and a configuration interaction including single excitations (CIS) in conjunction with 6-31G* and 6-31+G basis sets for extracting the force field of the excited states. The CIS procedure[21] proved to be very successful to describe the low-excited states dominated by single excitations of molecules such as benzene,[22] cyclopentadiene,[23] norbornadiene,[24] *B* state of polyenes,[25] imidazolium cation,[26] and oligomers of thiophene.[27] Semiempirical calculations indicate that also the S_1 and S_2 states of naphthalene belong to the group of excited molecular states which are well described by singly excited electronic configurations only. Thus we expect that the geometry changes of the states S_1 and S_2 with respect to S_0, which define the displacement parameters for the $S_0 \leftrightarrow S_1$ and $S_0 \leftrightarrow S_2$ transitions, are well described by the CIS procedure. Only when doubly excited configurations play a role in description of the electronic excited state, the use of CASSCF (MCSCF) method is called for to obtain reliable geometrical parameters, like in the S_1 states of azulene[28] and fulvene.[29] In addition to *ab initio* results, we present here the results of QCFF/PI+CIS(D) (Refs. 14, 15) calculations of the force fields and also use the CNDO/S +CIS Hamiltonian[16] in combination with the floating atomic orbitals method[30] to obtain vibronic coupling parameters which are pertinent to intensities of vibronic transition observed in the SVL fluorescence and excitation spectra of naphthalene.

Table I collects equilibrium geometries for the ground and lowest two excited singlet electronic states of naphthalene obtained with semiempirical and *ab initio* methods. These are compared with the experimental data (when available)[31,32] and with the results of recent CASSCF calculations.[19] It is seen that the electronic excitation to S_1 leads to a marked increase of the C_1C_6 and C_2C_3 bonds. QCFF/PI method underestimates somewhat these changes. Comparison with the CASSCF results[19] shows that very similar S_0-S_1 geometry changes are predicted by the latter and the CIS methods, in agreement with the fact that the S_1 wave function is dominated by single excitations. Upon excitation to S_2 the changes of individual geometrical parameters are smaller but since every bond length is subject to non-negligible changes the overall geometry change upon excitation to S_2 is larger than that of the S_1 state.

The calculated vertical electronic excitation energies are presented in Table II. The semiempirical energies are in close agreement with the experimentally observed origins of the $S_0 \rightarrow S_1(S_2)$ transitions $-3.97(4.45)$ eV.[10] The numbering of the excited states is according to their order obtained in QCFF/PI+CIS calculations. The *ab initio* CIS excitation energies are $\sim$1 eV too high which is a normal feature of CIS calculations especially when moderate basis sets are employed. In addition, the ordering of the closely lying S_1 and S_2 states is reversed, at variance with recent CASSCF calculations of excitation energies that predicted the correct order.[33] The inversion of states obtained by CIS calculations is probably indicative of the fact that, although the wave functions of these states are dominated by single excitations, the contribution of double excitations is somewhat larger for S_1,[33] which explains the correct result obtained at the CASSCF level. These two states form the L_b and L_a states of the perimeter model. The B_b and B_a states are S_5 and S_6, respectively. The calculated gap between the L and B states is roughly the same for semiempirical and *ab initio* methods and agrees quite well with the experiment.

The relevant feature of the S_1 state is its very weak transition dipole moment to S_0, a result of negative interference between the transition dipole moments of the two individual configurations that dominate its wave function. The sign of

TABLE IV. Vibrational frequencies (in cm^{-1}) of the in-plane normal modes (excluding CH stretches) in the $S_1(1B_{2u})$ state of naphthalene. Displacement parameters of the a_g modes for the $S_0 \rightarrow S_1$ transitions are also listed. Calculated CIS frequencies are scaled by 0.9.

	a_g				b_{3g}				b_{1u}				b_{2u}			
	QCFF	CIS1[a]	CIS2[b]	Expt.[c]	QCFF	CIS1	CIS2	Expt.	QCFF	CIS1	CIS2	Expt.	QCFF	CIS1	CIS2	Expt.
ν_{3a}	1552 (0.12)[d]	1562 (0.30)[e]	1542 (0.32)[f]	??	ν_{3b} 1631	1669	1661	1617	1480	1529	1516	1435	1445	1491	1482	??
ν_{4a}	1446 (0.12)	1452 (0.69)	1452 (0.59)	1434	ν_{4b} 1450	1442	1445	1365	1402	1384	1399	??	1225	1228	1239	1210
ν_{5a}	1397 (0.83)	1395 (1.10)	1394 (1.15)	1389	ν_{5b} 1281	1239	1261	1203	1316	1236	1252	1140	1148	1149	1167	??
ν_{6a}	1153 (0.11)	1146 (0.10)	1165 (0.13)	1150	ν_{6b} 1106	1110	1120	1166	1113	1095	1108	1088	1523	1615	1588	1555
ν_{7a}	1015 (0.45)	991 (0.34)	992 (0.47)	989	ν_{7b} 978	917	945	907	816	762	779	733	966	917	957	939
ν_{8a}	763 (0.73)	692 (0.87)	779 (0.97)	704	ν_{8b} 541	522	532	435	412	356	356	357	694	591	610	593
ν_{9a}	515(0.05)	493 (0.21)	503 (0.42)	503												

[a]6-31G* basis set.
[b]6-31+G basis set.
[c]Experiment, Ref. 9.
[d]QCFF/PI+CISD $S_0 \rightarrow S_1$ displacement parameter.
[e]HF/6-31G*-CIS/6-31G* $S_0 \rightarrow S_1$ displacement parameter.
[f]HF/6-31G*-CIS/6-31+G $S_0 \rightarrow S_1$ displacement parameter.

the $S_0 \leftrightarrow S_1$ dipole moment is of crucial importance to predict correctly the interference between contributions of HT and FC mechanisms to the intensity of TS vibronic bands. It has recently been shown that, although CNDO/S calculations give energies and state ordering in very good agreement with experimental data, they predict incorrectly the sign of the $S_0 \leftrightarrow S_1$ transition dipole moment.[34] *Ab initio* CIS calculations do better, and correctly predict the sign of the transition dipole moment. The calculated CIS/6-31+G ratio of transition dipole moments for the $S_0 \rightarrow S_i$ transitions is 1:37.5:157.4:90.3 for the $L_b:L_a:B_b:B_a$ states, respectively. Beside the sign, these ratios are important for assessing the relative importance of vibronically induced components of the vibronic transition dipole moments with respect to those produced by the $S_0 \rightarrow S_1$ transition dipole moment (*vide infra*).

Table III, collects the calculated vibrational frequencies of the in-plane normal modes of the ground electronic state. They are compared with the experimental values reported in Ref. 4. We have decided just to scale down the HF/6-31G* frequencies uniformly by a factor of 0.9 instead of scaling the force field by Pulay's procedure,[20] since previous calculations on other molecular systems indicated that scaling of the force-field affects little displacement parameters for an electronic transition.[29] The agreement between the calculated and experimental frequencies is satisfactory. We also list the displacement parameters of the a_g modes for the $S_1 \rightarrow S_0$ and $S_2 \rightarrow S_0$ transitions. These will be needed for the simulation of intensities of vibronic bands in the SVL spectra. It is seen that it is the ν_{5a} vibration, which is the CC stretching motion with a large amplitude on the C_1C_6 bond, that has the largest displacement parameter for both transitions, in accordance with the geometry change of both S_1 and S_2 states with respect to S_0. The second most Franck–Condon active mode for the $S_1 \rightarrow S_0$ transition is the ν_{8a} vibration which can be described as the ring breathing mode in which there is also a large participation of the C_1C_6 bond stretch. The ν_{9a} and ν_{3a} modes are instead the next most active vibrations for the $S_2 \rightarrow S_0$ transition. All other TS modes are only very weakly Franck–Condon active.

Tables IV, V, and VI contain the summary of the force field and displacement parameter calculations for the S_1 and S_2 states of naphthalene. The correlation of the excited state normal modes with those of ground state was established upon inspection of the Dushinsky matrices which give projections of one set of modes onto the other. QCFF/CI+CISD, CIS/6-31G*, and CIS/6-31+G frequencies of the in-plane modes and the corresponding displacement parameters of the

TABLE V. Vibrational frequencies (in cm^{-1}) of the in-plane normal modes (excluding CH stretches) in the $S_2(1B_{1u})$ state of naphthalene. Displacement parameters of the a_g modes for the $S_0 \rightarrow S_2$ transitions are also listed. Calculated CIS frequencies are scaled by 0.9.

	a_g		b_{3g}		b_{1u}		b_{2u}	
	QCFF	CIS[a]	QCFF	CIS	QCFF	CIS	QCFF	CIS
ν_{3a}	1589 (0.66)[b]	1533 (0.37)[c]	ν_{3b} 1402	1370	1447	1466	1534	1524
ν_{4a}	1483 (0.20)	1444 (0.01)	ν_{4b} 1490	1415	1412	1387	1402	1314
ν_{5a}	1365 (1.33)	1302 (1.66)	ν_{5b} 1277	1197	1337	1253	1148	1131
ν_{6a}	1154 (0.12)	1137 (0.58)	ν_{6b} 1053	993	1092	1057	1207	1158
ν_{7a}	1053 (0.38)	1020 (0.50)	ν_{7b} 965	890	831	781	1004	959
ν_{8a}	788 (0.21)	716 (0.24)	ν_{8b} 532	455	404	347	692	572
ν_{9a}	514 (0.58)	485 (0.94)						

[a]6-31G* basis set.
[b]QCFF/PI+CISD $S_0 \rightarrow S_2$ displacement parameter.
[c]HF/6-31G*-CIS/6-31G* $S_0 \rightarrow S_2$ displacement parameter.

TABLE VI. Displacement parameters of the a_g modes for the $S_1 \rightarrow S_2$ and $S_2 \rightarrow S_1$ transitions.

	$S_2 \rightarrow S_1$		$S_1 \rightarrow S_2$	
ν_{3a}	1552[a] (0.84)[b]	1562[c] (0.99)[d]	1589[e] (0.88)[f]	1533[g] (0.70)[h]
ν_{4a}	1446 (0.02)	1452 (0.22)	1483 (0.08)	1444 (0.32)
ν_{5a}	1397 (0.55)	1395 (0.11)	1365 (0.56)	1302 (0.47)
ν_{6a}	1153 (0.23)	1146 (0.46)	1154 (0.24)	1137 (0.55)
ν_{7a}	1015 (0.23)	991 (0.13)	1053 (0.12)	1020 (0.07)
ν_{8a}	763 (0.48)	692 (0.62)	788 (0.49)	716 (0.62)
ν_{9a}	515 (0.65)	493 (0.71)	514 (0.64)	485 (0.73)

[a] S_1 frequency computed with the QCFF/PI+CISD method.
[b] QCFF/PI+CISD $S_2 \rightarrow S_1$ displacement parameter.
[c] S_1 frequency (scaled by a factor of 0.9) computed at *ab initio* CIS/6-31G* level.
[d] *Ab initio* $S_2 \rightarrow S_1$ displacement parameter.
[e] S_2 frequency computed with the QCFF/PI+CISD method.
[f] QCFF/PI+CISD $S_1 \rightarrow S_2$ displacement parameter.
[g] S_2 frequency (scaled by a factor of 0.9) computed at *ab initio* CIS/6-31G* level.
[h] *Ab initio* $S_1 \rightarrow S_2$ displacement parameter.

a_g modes for the $S_0 \rightarrow S_1$, $S_0 \rightarrow S_2$, and $S_1 \leftrightarrow S_2$ transitions, that will be used in the simulations of the spectra, are given. The experimental frequencies of S_1 were taken from Ref. 9. The *ab initio* frequencies are again scaled uniformly by a factor of 0.9. As for the emission, the most Franck–Condon active modes in $S_0 \rightarrow S_1$ absorption are again the ν_{5a} and ν_{8a} modes. However, there is some modest mode mixing among the CC stretching modes as evidenced by increased displacement parameters of the ν_{3a} and ν_{4a} modes. Mode mixing is stronger upon excitation to S_2, and thus the largest activity in the $S_0 \rightarrow S_2$ absorption is computed, according to the *ab initio* calculations, not only for ν_{5a} and ν_{9a}, but also for the ν_{6a} and ν_{7a} modes. The size of this mixing is made evident by the Dushinsky matrices of the a_g modes for the S_2 and S_1 states with respect to S_0, presented in Table VII. The frequencies of the b_{3g} modes in the S_1 state are well reproduced by the calculation with the exception of the ν_{8b} mode, which deviates from the experimental value by ~ 90 cm^{-1}. This is the largest discrepancy among the frequencies of the in-plane modes for the L_b state. There is a simple explanation for the computed deviation; the ν_{8b} mode couples quite strongly the S_1 with the S_2 state (see below), and because of the incorrect order of the S_1 state as predicted by the CIS method, the coupling leads to an increase of such frequency instead of a decrease, as compared to the ground state frequency. This discrepancy diminishes somewhat for the MC-SCF method[19] since the order of states is correct at this level of theory.

Table VIII shows the Dushinsky matrix for the b_{3g} modes indicating excellent preservation of the identities of the individual modes upon excitation to the S_1 state. Much stronger mixing characterizes the b_{3g} modes of S_2; in particular, the frequency of the ν_{3b} mode is computed to be smaller than that of the ν_{4b} mode. This frequency inversion is probably an artifact of the CIS calculation which results from the reversed order of S_1 and S_2, since the latter mode also couples considerably the two states. Among in-plane modes of other symmetries it is interesting to notice that the b_{2u} mode with the frequency of 1144 cm^{-1} in the S_0 state correlates with the b_{2u} mode with the frequency of 1555 cm^{-1} in the S_1 state. This dramatic increase of the frequency of this vibration results from its strong vibronic activity in coupling the S_0 and S_1 states. In this respect this mode is an analog of the ν_{14} mode of benzene.

Since the dipole moment of the $S_0 \rightarrow S_1$ transition is very small, the borrowing of intensity from the $S_0 \rightarrow S_i$, $i=2,5,6$ transitions will play a major role in the vibronic structure of the SVL spectra in naphthalene. This borrowing takes place via a_g (S_1-S_5 coupling) and b_{3g} (S_1-S_2 and S_1-S_6 couplings) modes. To calculate the strengths of the relevant couplings we used both the QCFF/PI+CISD and CIS/6-31G* modes of the S_1 state and the CNDO/S+CIS electronic

TABLE VII. Dushinsky matrices for the rotation of a_g normal coordinates of S_1 and S_2 with respect to the S_0 state, computed at the HF/6-31G*(S_0) and CIS/6-31G*(S_1,S_2) *ab initio* level.

S_0 \ S_1	1562	1452	1395	1146	991	692	493
1605	0.934	−0.087	−0.326	0.052	0.090	−0.054	⋯
1463	0.203	0.925	0.316	⋯	⋯	⋯	⋯
1338	0.277	−0.363	0.875	−0.101	0.061	0.107	⋯
1158	⋯	⋯	0.120	0.983	0.127	⋯	⋯
1005	−0.03	0.059	⋯	−0.129	0.983	−0.063	⋯
748	⋯	⋯	−0.113	⋯	0.068	0.987	−0.079
496	⋯	⋯	⋯	⋯	⋯	0.077	0.996
S_0 \ S_s	1533	1444	1302	1137	1020	716	485
1605	0.782	0.545	−0.228	0.084	0.177	⋯	⋯
1463	−0.603	0.763	−0.207	0.093	⋯	⋯	⋯
1338	−0.090	−0.325	−0.916	⋯	0.197	0.071	⋯
1158	⋯	0.109	−0.145	−0.945	−0.266	⋯	⋯
1005	−0.118	⋯	0.198	−0.298	0.926	⋯	⋯
748	⋯	⋯	0.057	⋯	⋯	0.993	−0.090
496	⋯	⋯	0.050	⋯	⋯	0.088	0.994

TABLE VIII. Dushinsky matrices for the rotation of b_{3g} normal coordinates of S_1 and S_2 with respect to the S_0 state, computed at the HF/6-31G*(S_0) and CIS/6-31G*(S_1,S_2) *ab initio* level.

S_0 \ S_1	1669	1442	1239	1110	917	522
1660	0.970	0.218	−0.072	0.069	⋯	⋯
1461	−0.223	0.971	⋯	0.082	⋯	⋯
1235	0.078	⋯	0.988	−0.133	⋯	⋯
1146	⋯	−0.094	0.137	0.985	⋯	⋯
920	⋯	⋯	⋯	⋯	0.988	⋯
499	⋯	⋯	⋯	⋯	⋯	0.999
S_0 \ S_2	1370	1415	1197	993	890	455
1660	−0.877	−0.083	0.176	0.428	0.099	⋯
1461	−0.083	0.983	−0.129	0.083	−0.055	⋯
1235	0.197	0.139	0.968	⋯	0.057	⋯
1146	0.424	⋯	−0.109	0.894	0.064	⋯
920	⋯	0.056	−0.076	−0.098	0.990	⋯
499	⋯	⋯	⋯	⋯	⋯	−0.998

states.[16] The resulting vibronic coupling parameters are collected in Table IX. There is an overall agreement between the two sets of vibronic coupling parameters with the exception of the parameter for the ν_{ia}, $i=3,4,5$ modes. For the QCFF/PI modes, the coupling is concentrated in the ν_{3a} mode, while it is spread more evenly over the three *ab initio* modes. It is easy to see at the same time that the overall strength of the coupling is almost the same for the three modes in the two sets of normal coordinates (170 cm^{-1} and 165 cm^{-1} for the CIS/6-31G* and QCFF/PI+CISD modes, respectively). Thus the source of the noted redistribution of the coupling strength is the mixing of *ab initio* normal modes upon excitation to the S_1 state (see Table IV). This mixing is negligible for the QCFF/PI modes. It is evident that the most important couplings for the vibronic structure of the SVL spectra are those between the L_b state and the two B states. This stems from very large transition dipole moments between the ground state and the B states. From the couplings presented in Table IX it is seen that the two lowest frequency modes of each symmetry species seem to be the most active. The ν_{9a} and ν_{8a} modes describe elongation motions of the rings along the long and short molecular axes, respectively, while the ν_{8b} and ν_{7b} modes describe the CCC deformations of the rings. The strong vibronic activity of the ν_{9a} mode, coupled with its small displacement, indicates that intensities of the vibronic lines that arise from a change in the vibrational quantum number of this mode will be mostly governed by vibronic coupling, similarly to the lines in which b_{3g} modes change its quantum number by one. For other TS modes, in particular the ν_{8a} and ν_{5a}, the interference between the Franck–Condon and vibronic mechanisms will be of the utmost importance in determining vibronic intensities of the SVL lines resulting from a change of vibrational excitation of these modes.

TABLE IX. The calculated vibronic coupling strengths, $V_{S_iS_j}$ (in cm^{-1}), between the CNDO/S+CIS states for the a_g and b_{3g} modes of naphthalene.

	ω	$V_{S_1S_5}$	$V_{S_1S_2}$	$V_{S_1S_6}$
ν_{3a}	1562[a] (1552)[b]	−93[c] (−34)[d]	⋯	⋯
ν_{4a}	1452 (1446)	−90 (−21)	⋯	⋯
ν_{5a}	1395 (1397)	−110 (−160)	⋯	⋯
ν_{6a}	1146 (1153)	34 (12)	⋯	⋯
ν_{7a}	991 (1015)	25 (29)	⋯	⋯
ν_{8a}	692 (763)	140 (121)	⋯	⋯
ν_{9a}	493 (515)	−161 (−155)	⋯	⋯
ν_{3b}	1669 (1631)	⋯	−75 (−61)	80 (70)
ν_{4b}	1442 (1450)	⋯	−8 (−14)	−47 (−45)
ν_{5b}	1239 (1281)	⋯	−9 (−2)	64 (56)
ν_{6b}	1110 (1106)	⋯	−18 (−21)	18 (17)
ν_{7b}	917 (978)	⋯	−45 (−35)	−193 (−159)
ν_{8b}	522 (541)	⋯	−56 (−44)	−374 (−352)

[a]CIS/6-31G* vibrational frequency of the S_1 state.
[b]QCFF/PI+CISD vibrational frequency of the S_1 state.
[c]Coupling for the CIS/6-31G* S_1 state mode.
[d]Coupling for the QCFF/PI+CISD S_1 state mode.

We have determined the induced intensities of the b_{3g} fundamentals in the $S_0 \rightarrow S_1$ spectrum by calculating the change of the transition dipole moment as the molecule is distorted along one of the b_{3g} S_0 state normal coordinates. Diabatic QCFF/PI+CISD normal modes and CNDO/S+CIS

TABLE X. Calculated (CNDO/S) induced dipole moments, M_i, and oscillator strengths, f_i, by the b_{3g} modes for the $S_0 \rightarrow S_1$ transition in naphthalene.

Mode	M_i		$f_i \times 10^{-5}$		
origin	0.051 36[a]	0.032 79[b]	93.0[a]	37.0[b]	…[c]
ν_{8b}	0.025 91	0.016 85	23.8	9.8	32.9
ν_{7b}	0.014 78	0.007 46	7.7	1.9	10.0
ν_{6b}	0.004 53	0.000 23	0.7	0.0	2.5
ν_{5b}	0.005 31	0.002 14	1.0	0.2	0.1
ν_{4b}	0.008 37	0.002 82	2.5	0.3	2.2
ν_{3b}	0.010 84	0.001 70	4.2	0.1	4.2

[a]CIS calculation.
[b]CISD calculation.
[c]Reference 13.

method were used to this purpose. The result is presented in Table X, where it is compared with the calculations of Robey *et al.*[13] It is seen that the calculation predict the ν_{8b} mode to form the strongest false origin in the absorption spectrum; the false origin induced by the ν_{7b} mode being the second strongest. This agrees nicely with the experimental results of SGK.[5] As already pointed out by Robey *et al.*,[13] when compared to the intensity of the 0–0 transition, the induced activity predicted by CNDO/S calculations appears to be underestimated. Robey *et al.* concluded that the oscillator strength predicted by CNDO/S for the $S_0 \rightarrow S_1$ transition was overestimated by at least a factor of 10, as a consequence of the very subtle balance between the transition dipole moments of the two configurations dominating S_1. These early indications are in keeping with our choice of using, in the model described in the next sections, *ab initio* transition dipole moments instead of those computed with CNDO/S.

III. VIBRONIC INTENSITIES

To evaluate the intensity of vibronic bands, originated by both FC and HT mechanisms, we adopted the perturbative approach described in Ref. 18. Here, we extend the method to include vibronic coupling effects for TS modes, in order to describe the interference of the vibronically induced (HT) and the allowed (FC) intensity contributions to the TS bands.

We label $|L;v_a^L;v_s^L)$ a perturbed, non-BO vibronic eigenfunction of a molecular state resulting from the diabatic $|L^0\rangle|v_a^L)|v_s^L)$ state. $|v_{a,s}^L)$ is a shorthand to represent the product of NTS and TS vibrational wave functions $\Pi_{i_a}^{\mathrm{NTS}}|v_{i_a}^L)$, $\Pi_{i_s}^{\mathrm{TS}}|v_{i_s}^L)$, respectively. The expansion of the vibronic state reads

$$
\begin{aligned}
|L;v_a^L;v_s^L) = |L^0\rangle \prod_{i_a}^{\mathrm{NTS}} |v_{i_a}^L) \prod_{i_s}^{\mathrm{TS}} |v_{i_s}^L) + \sum_{j_a} \sum_{N\neq L} \sum_{v_a^N} \sum_{v_s^N} \frac{V_{j_a}^{L,N}}{\Delta E^{L,N}} (v_{j_a}^N|Q_{j_a}|v_{j_a}^L) \prod_{i_a\neq j_a}^{\mathrm{NTS}} (v_{i_a}^N|v_{i_a}^L) \prod_{i_s}^{\mathrm{TS}} (v_{i_s}^N|v_{i_s}^L) \\
\cdot |N^0\rangle|v_{j_a}^N) \prod_{i_a\neq j_a}^{\mathrm{NTS}} |v_{i_a}^N) \prod_{i_s}^{\mathrm{TS}} |v_{i_s}^N) + \sum_{j_s} \sum_{P\neq L} \sum_{v_a^P} \sum_{v_s^P} \frac{V_{j_s}^{L,P}}{\Delta E^{L,P}} (v_{j_s}^P|Q_{j_s}|v_{j_s}^L) \prod_{i_a}^{\mathrm{NTS}} (v_{i_a}^P|v_{i_a}^L) \prod_{i_s\neq j_s}^{\mathrm{TS}} (v_{i_s}^P|v_{i_s}^L) \\
\cdot |P^0\rangle|v_{j_s}^P) \prod_{i_a}^{\mathrm{NTS}} |v_{i_a}^P) \prod_{i_s\neq j_s}^{\mathrm{TS}} |v_{i_s}^P),
\end{aligned}
\tag{1}
$$

where

$$
\Delta E^{L,N} = E_L^0 - E_N^0 + \sum_{i_s}^{\mathrm{TS}} (v_{i_s}^L \omega_{i_s}^L - v_{i_s}^N \omega_{i_s}^N) + \sum_{i_a}^{\mathrm{NTS}} (v_{i_a}^L \omega_{i_a}^L - v_{i_a}^N \omega_{i_a}^N) \tag{2}
$$

is the energy difference, in $\hbar$ units, between the two vibronic states interacting through the adiabatic coupling integral

$$
V_{i_{s,a}}^{L,N} = \left\langle L^0 \left| \left(\frac{\partial U}{\partial Q_{i_{s,a}}} \right)_0 \right| N^0 \right\rangle \tag{3}
$$

and

$$
\sum_{v_{s,a}^L} = \sum_{v_{(1)_{s,a}}^L} \sum_{v_{(2)_{s,a}}^L} \cdots \sum_{v_{(\mathrm{TS,NTS})_{s,a}}^L} \tag{4}
$$

with $v_{(1)_{s,a}}^L + v_{(2)_{s,a}}^L + \cdots + v_{(\mathrm{TS,NTS})_{s,a}}^L = v_{s,a}^L$. The adiabatic coupling integrals, or vibronic coupling parameters, were calculated by the quantum-chemical methods as discussed in the previous section, and are given in Table IX.

The general expression of the transition dipole moment between two vibronic states $|G;v_a^G;v_s^G)$ and $|L;v_a^L;v_s^L)$ is then

$$(G;v_a^G;v_s^G|\mu|L;v_a^L;v_s^L)=\langle G^0|\mu|L^0\rangle\prod_{i_a}^{\mathrm{NTS}}(v_{i_a}^G|v_{i_a}^L)\prod_{i_s}^{\mathrm{TS}}(v_{i_s}^G|v_{i_s}^L)+\sum_{j_a}^{\mathrm{NTS}}\sum_{N\neq L}\sum_{v_a^N}\sum_{v_s^N}\frac{V_{j_a}^{L,N}}{\Delta E^{L,N}}\langle G^0|\mu|N^0\rangle(v_{j_a}^G|v_{j_a}^N)$$
$$\times(v_{j_a}^N|Q_{j_a}|v_{j_a}^L)\cdot\prod_{i_a\neq j_a}^{\mathrm{NTS}}(v_{i_a}^G|v_{i_a}^N)(v_{i_a}^N|v_{i_a}^L)\prod_{i_s}^{\mathrm{TS}}(v_{i_s}^G|v_{i_s}^N)(v_{i_s}^N|v_{i_s}^L)$$
$$+\sum_{j_s}^{\mathrm{TS}}\sum_{P\neq L}\sum_{v_a^P}\sum_{v_s^P}\frac{V_{j_s}^{L,P}}{\Delta E^{L,P}}\langle G^0|\mu|P^0\rangle(v_{j_s}^G|v_{j_s}^P)(v_{j_s}^P|Q_{j_s}|v_{j_s}^L)\cdot\prod_{i_s\neq j_s}^{\mathrm{TS}}(v_{i_s}^G|v_{i_s}^P)(v_{i_s}^P|v_{i_s}^L)\prod_{i_a}^{\mathrm{NTS}}(v_{i_a}^G|v_{i_a}^P)$$
$$\times(v_{i_a}^P|v_{i_a}^L)+\sum_{j_a}^{\mathrm{NTS}}\sum_{M\neq G}\sum_{v_a^M}\sum_{v_s^M}\frac{V_{j_a}^{G,M}}{\Delta E^{G,M}}\langle M^0|\mu|L^0\rangle(v_{j_a}^G|Q_{j_a}|v_{j_a}^M)(v_{j_a}^M|v_{j_a}^L)\cdot\prod_{i_a\neq j_a}^{\mathrm{NTS}}(v_{i_a}^G|v_{i_a}^M)$$
$$\times(v_{i_a}^M|v_{i_a}^L)\prod_{i_s}^{\mathrm{TS}}(v_{i_s}^G|v_{i_s}^M)(v_{i_s}^M|v_{i_s}^L)+\sum_{j_s}^{\mathrm{TS}}\sum_{O\neq G}\sum_{v_a^O}\sum_{v_s^O}\frac{V_{j_s}^{G,O}}{\Delta E^{G,O}}\langle O^0|\mu|L^0\rangle(v_{j_s}^G|Q_{j_s}|v_{j_s}^O)(v_{j_s}^O|v_{j_s}^L)$$
$$\cdot\prod_{i_s\neq j_s}^{\mathrm{TS}}(v_{i_s}^G|v_{i_s}^O)(v_{i_s}^O|v_{i_s}^L)\prod_{i_a}^{\mathrm{NTS}}(v_{i_a}^G|v_{i_a}^O)(v_{i_a}^O|v_{i_a}^L). \tag{5}$$

The first term in Eq. (5) describes the FC contribution to the intensity. The second and fourth terms represent the HT contribution induced by the coupling mediated by NTS modes, of the final $|L^0\rangle|v_a^L\rangle|v_s^L\rangle$ and initial $|G^0\rangle|v_a^G\rangle|v_s^G\rangle$ vibronic states, respectively, with other electronic states. Finally, the third and fifth terms in Eq. (5) describe the analogous contribution induced by the activity of TS modes.

Equation (5) can be used to model vibronic intensities in case of weak vibronic coupling and, in the form presented above, in the absence of Dushinsky rotation.[35] Within the harmonic approximation, the overlap $(v_{i_{a,s}}^P|v_{i_{a,s}}^Q)$ between vibrational wave functions of the states P and Q, is computed by using recursion formulas.[36] These require the knowledge of vibrational frequencies ω_i in the two electronics states P and Q, and the displacement parameter B_i for the ith mode, which is defined as

$$B_i=\left(\frac{\omega_i}{\hbar}\right)^{1/2}Q_{iP}^{P,Q}. \tag{6}$$

Here $Q_{iP}^{P,Q}$ is the projection of the expressed in Cartesian coordinates geometry change between the two states onto the P-state normal coordinate Q_i^P, that is

$$Q_{iP}^{P,Q}=[\mathbf{x}_Q-\mathbf{x}_P]\mathbf{M}^{1/2}\mathbf{L}_i^P, \tag{7}$$

where $\mathbf{x}_K$ is the $3N$ dimensional vector of the equilibrium Cartesian coordinates in the Kth state, $\mathbf{M}$ is the $3N\times 3N$ diagonal matrix of the atomic masses, and $\mathbf{L}_i^P$ is the $3N$ vector describing the normal coordinate Q_i^P, in terms of mass-weighted Cartesian coordinates.

As indicated by Eq. (5), to simulate the intensity of a vibronic band, overlap integrals of TS modes for various pairs of electronic states have to be evaluated. In the simplest case, of pure FC mechanism, the displacement parameters for the $S_1\rightarrow S_0$ (emission spectrum) and the $S_0\rightarrow S_1$ (absorption spectrum) transitions are required. When contributions from the HT mechanism due to vibronic coupling of S_1 with the S_n state are included, the displacement parameters for the $S_0\rightarrow S_n$ and $S_n\rightarrow S_1$ transitions are also requested. These displacements were calculated by quantum-chemical methods, as described in the previous section, and are collected in Tables III, IV and V and VI.

Under the additional assumption of equal $\omega_{i_{a,s}}$ frequencies in every electronic state, the value of vibrational overlaps for NTS modes is reduced to the simple expression $(v_{i_a}^P|v_{i_a}^Q)=\delta_{v_{i_a}^P,v_{i_a}^Q}$. Integrals of the type $(v_{i_{a,s}}^P|Q_{i_{a,s}}|v_{i_{a,s}}^Q)$ in Eq. (5) are computed with the help of the recursion formulas for eigenfunctions of the harmonic oscillator,[37]

$$(v_{i_{a,s}}^P|Q_{i_{a,s}}|v_{i_{a,s}}^Q)=\sqrt{\left(\frac{\hbar}{\omega_{i_{a,s}}}\right)\frac{v_{i_{a,s}}^Q}{2}}\,(v_{i_{a,s}}^P|v_{i_{a,s}}^Q-1)$$
$$+\sqrt{\left(\frac{\hbar}{\omega_{i_{a,s}}}\right)\frac{v_{i_{a,s}}^Q+1}{2}}\,(v_{i_{a,s}}^P|v_{i_{a,s}}^Q+1). \tag{8}$$

For NTS modes the above relation simplifies to

$$(v_{i_a}^P|Q_{i_a}|v_{i_a}^Q)=\sqrt{\left(\frac{\hbar}{\omega_{i_{a,s}}}\right)\frac{v_{i_a}^Q}{2}}\,\delta_{v_{i_a}^P,v_{i_a}^Q-1}$$
$$+\sqrt{\left(\frac{\hbar}{\omega_{i_{a,s}}}\right)\frac{v_{i_a}^Q+1}{2}}\,\delta_{v_{i_a}^P,v_{i_a}^Q+1}, \tag{9}$$

which reduces sums of the type $\Sigma_{v_a^K}^{\mathrm{NTS}}$ in Eq. (5) to only two terms.

In the present study we analyze absorption and SVL fluorescence spectra hence, the initial vibronic

states will be of the type $|S_0;\ \Pi_{i_a}^{\mathrm{NTS}}|0_{i_a}^{S_0})\Pi_{i_s}^{\mathrm{TS}}|0_{i_s}^{S_0})$, $|S_1;\Pi_{i_a}^{\mathrm{NTS}}|0_{i_a}^{S_1})\Pi_{i_s}^{\mathrm{TS}}|0_{i_s}^{S_1})$, $|S_1;|1_{j_a}^{S_1})\Pi_{i_a\neq j_a}^{\mathrm{NTS}}|0_{i_a}^{S_1})\Pi_{i_s}^{\mathrm{TS}}|0_{i_s}^{S_1})$ or $|S_1;\Pi_{i_a}^{\mathrm{NTS}}|0_{i_a}^{S_1})1_{j_s}^{S_1})\Pi_{i_s\neq j_s}^{\mathrm{TS}}|0_{i_s}^{S_1})$.

IV. SIMULATED SVL FLUORESCENCE AND ABSORPTION SPECTRA

The formalism of Sec. III was used to produce the SVL spectra from vibronic levels of the S_1 manifold as well as the $S_0 \rightarrow S_1$ absorption spectrum.

The model adopted to simulate the spectra includes, beside the ground state S_0, the four excited electronic states S_1, S_2, S_5, and S_6. The displacement parameters required to evaluate overlaps among vibrational levels of S_0, S_1, and S_2, were computed by quantum-chemical methods and are presented in the tables. The displacement parameters necessary to estimate overlaps involving the vibrational levels of S_5 and S_6, were obtained by assuming the geometry of S_5 equal to the geometry of S_1, and the geometry of S_6 identical to that of S_2. The latter assumption is based on the fact that the two pairs of states are described by the same electronic excitations. In addition, since vibronic coupling parameters involving the ground state were computed to be negligible, only couplings of the S_1 state with higher excited states were included in the model. Finally, to simplify the comparison with experimental spectra, the simulations were performed by using experimental vibrational frequencies. The remaining input parameters for the simulations were taken form the quantum-chemical calculations presented in Sec. II. Rather than adjust each parameter separately, we opted for a ''global'' adjustment of the parameters to correct for the obvious deficiencies of the quantum-chemical calculations and for the approximations adopted in the model. In this way we hoped to obtain a good qualitative agreement with a number of experimental spectra.[5,10,11] We set the ratios of the transition dipole moments to the S_1, S_2, S_5, and S_6 states as 1:40:200:130 which is close to the CIS/6-31+G calculated ratios (see Sec. II). We find then that, in order to properly describe the induced intensities of the b_{3g} fundamentals, we have to scale the calculated vibronic coupling parameters up by a factor of 2.4. In view of the small values of the calculated coupling parameters, this scaling does not seem to be unexpected. This is further supported by the ratio of the induced intensity of the ν_{8b} fundamental with the intensity of the origin of the $S_0 \rightarrow S_1$ transition, computed by using the method described in Sec. II (Table X), which is far too small as compared with the experiment. Such scaling would put the oscillator strength of this false origin at ~0.001 37 which is very close to the observed value of 0.001 32.[5] For the false origin induced by the ν_{7b} mode the corresponding numbers are then 0.000 44 (computed) vs 0.000 55 (experimental). The intensities presented in Table X were obtained from a CI calculation that included many more excited states beside the S_1, S_2, S_5, and S_6 selected for the simulation described here. We have verified that in the case of mode ν_{7b}, its intensity is induced not only by the coupling of S_1 with S_2 and S_6, but also by the coupling with higher B_{1u} excited states. In fact, the slight underestimate of the intensity of this false origin computed by the method of Sec. II (see above) can be ascribed to truncation effects due to the incomplete CI space. To account for this in the simulations of the spectra presented below, we have changed S_1-S_6 coupling strength, $V_7^{1,6}$, from -192 cm^{-1} to -260 cm^{-1}, before scaling all coupling parameters of the b_{3g} modes (Table IX) by 2.4. The calculated coupling parameters of the TS modes were scaled by a factor of 3.

We have performed two sets of simulations. In the first one (set I), we assumed that no mode mixing occurs in the excited states, i.e., all modes retain fully their identity upon electronic excitation. In the second set (set II), we took mode mixing of the TS modes into account, by using the coefficients calculated for the CIS/6-31 G* vibrational normal coordinates (see Table VII). As Table VIII shows, the mixing is not important for the b_{3g} modes. The displacement parameters utilized in the calculation have slightly altered values of the HF/6-31G*–CIS/6-31G* calculations (Tables III and IV). We decreased the displacement parameter of the ν_{9a} mode, relative to the $S_0 \leftrightarrow S_1$ transition, by 0.1 (from 0.24 to 0.14) and then scaled all calculated displacement parameters by a factor of 0.9. In set I, which ignores mixing of the ν_{3a}, ν_{4a}, and ν_{5a} modes (Table VII), the displacement parameters for the $S_0 \leftrightarrow S_1$ and $S_0 \leftrightarrow S_2$ transitions of the last two modes, were increased and decreased by 0.42, respectively. In addition the couplings $V_4^{1,5}$ and $V_5^{1,5}$ were changed, before scaling, from -90 to -129 cm^{-1} and from -110 to -70 cm^{-1}, respectively. These changes reflect two-dimensional rotation of the ν_{4a} and ν_{5a} coordinates upon excitation to the S_1 state. In set II, no modification of the *ab initio* computed parameters was performed, but the three-coordinate rotation, as given in Table VII, was taken explicitly into account. It was assumed that the same rotation of normal coordinates occurs upon excitation to S_1 and S_5. In analogy, identical mode mixing was assumed for the S_2 and S_6 pair of states. It was found for both sets that the intensity of the $(\nu_{9a})_0^1$ and $(\nu_{9a})_1^0$ fundamentals was much stronger than the experimentally observed value. To bring it into closer agreement with the experiment we scaled the the vibronic coupling for this mode by a factor of 1.1 instead of a factor of 3, as we did for all other TS modes. Due to the lack of space, we present here only the figures of the spectra calculated with set I of parameters. Those corresponding to set II are available via PAPS.[38] We discuss individual spectra separately.

A. 0_0^0 emission spectrum

Figures 1(a) and 1(b) present the calculated (set I) and observed[5] emission spectra. The calculated spectrum for set II of parameters is available via PAPS [Fig. 1(c)]. The dominant line of the spectrum is the fundamental of the ν_{8b} mode, which is ~14 (6) times as intense as the origin of the spectrum, for set I(II), respectively. This should be compared to a factor of 10 or 8.2 given by SGK.[5] This ratio is very sensitive to exact nature of mixing among the TS modes, since this mixing affects strongly the (weak) intensity of the origin of the spectrum both via the FC and the HT mechanisms. The calculated intensity of the ν_{9a} fundamental which is

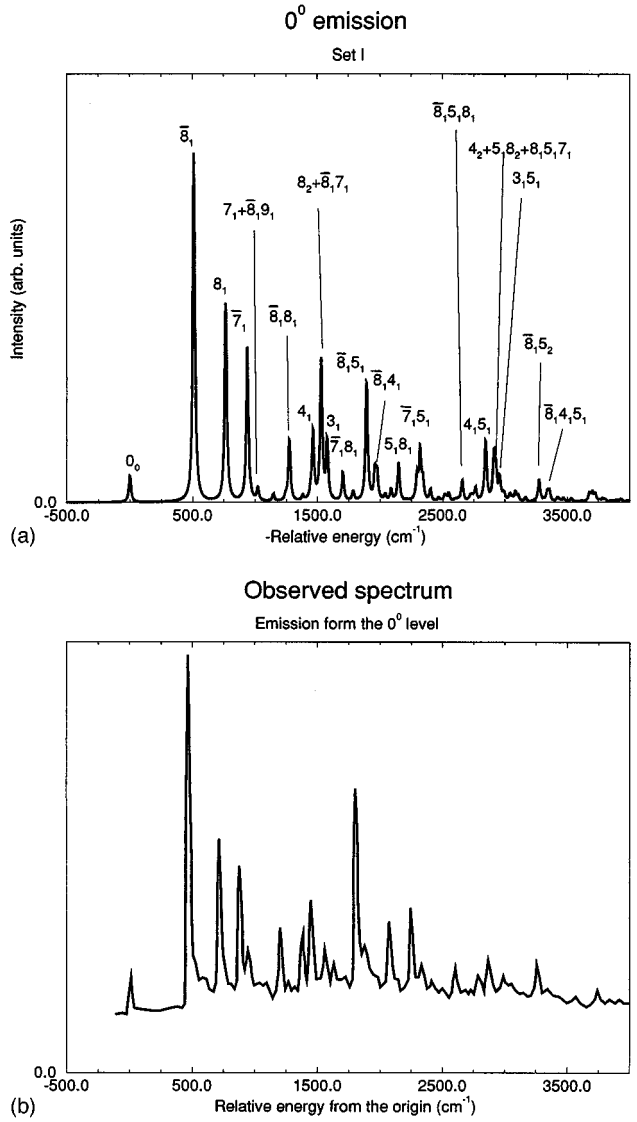

FIG. 1. Calculated (a, set I) and observed (b, after Ref. 5) emission spectrum from the 0^0 level. The linewidth used in simulation is 10 cm^{-1}.

quasidegenerate with that of the ν_{8b} mode is found to contribute by a factor of 1/15 to the band at $\sim$510 cm^{-1} in the emission spectrum. Due to near degeneracy of the frequencies of the ν_{8b} and ν_{9a} modes in the ground electronic state, lines belonging to transitions to the one-quantum level of the ν_{8b} mode get small contributions form transitions to the one-quantum level of the ν_{9a} vibration. The relative intensity (with respect to the origin) of the ν_{8a} fundamental is 7.7(2.8) for the sets I(II), respectively, while the value reported by SGK is 4.6, e.g., similar agreement as for the ν_{8b} fundamental. The calculations predict also considerable intensity for the ν_{7b} fundamental (6.1 and 2.7 vs observed 3.4), reproduce the observed small intensity of the ν_{7a} fundamental and the observed intensity of the $(\nu_{8a})_1^0(\nu_{8b})_1^0$ combination band. The marked difference between the two calculated emission spectra occurs in the region of 1500 cm^{-1} below the origin, where there are three closely lying bands belonging to ν_{4a}, ν_{3a} fundamentals and the sum of the ν_{8a} overtone plus the $(\nu_{8b})_1^0(\nu_{7a})_1^0$ combination band. Both sets predict marked intensity for the $(\nu_{8a})_2^0$ line at 1530 cm^{-1} below the origin. With the displacement parameters described above, the intensity of the $(\nu_{8b})_1^0(\nu_{7a})_1^0$ combination band is predicted to be almost negligible. However, by slightly increasing the B_{7a} of the $S_0 \leftrightarrow S_2$ and $S_1 \leftrightarrow S_2$ transitions by 0.5 and 0.1, respectively, the intensity of the combination band reaches the same magnitude of the ν_{8a} overtone. The contribution of the latter band was previously proposed by us on the basis of simple one-mode calculations.[6] The difference between the spectra resulting from the two sets is evident in quite different intensities of the ν_{4a} and ν_{3a} fundamentals; set I predicts two strong bands for the two fundamentals, while set II shows weak intensities. The experimental spectrum shows a strong ν_{4a} fundamental and a weak ν_{3a} fundamental. The result of the simulations indicates that the intensities of TS fundamentals involved in Dushinsky rotation are very sensitive to the exact amount of mode mixing. Present *ab initio* methods seems to be not accurate enough to describe this mixing in a quantitative way. Other controlling factors can, however, partially account for the difference between predicted and experimental intensities. It must be recalled that the model includes quite a small number of electronic states and is based on precise approximations on the geometry and vibrational mode mixing of the excited states S_5 and S_6. The result of the simulations appears to indicate that the assumption of structure and modes of the latter states identical to those of S_1 and S_2 respectively is probably oversimplified to describe quantitatively the details of the spectra. Indeed, small changes in the displacement parameters of S_6 with respect to S_2 may lead to different intensity ratios for the various vibronic bands. The computational effort required to obtain reliable optimized geometries and vibrational force fields for excited states higher than S_2 is beyond the computational resources presently available to us, but we are confident that a deep analysis of the factors governing the vibrational structure of the spectra can be obtained with the model adopted here. The calculations predict short Franck–Condon progression built upon each line by the ν_{5a} mode in agreement with the assignments proposed by SGK. The overall description of the spectrum is closer to experiment with set I of parameters, a fact that tends to support the conclusion that the lack of Dushinsky mixing and the other approximations introduced in the model can be partially overcome by a slight modification of the *ab initio* computed parameters.

B. Absorption spectrum

Figure 2(a) shows the calculated (set I) absorption spectrum [set II available from PAPS, Fig. 2(c)] which should be compared with the fluorescence excitation spectrum taken from Ref. 10 and presented in Fig. 2(b). Set II is somewhat superior in reproducing intensities of individual vibronic lines. Both sets underestimate the intensity of the $(\nu_{8b})_0^1(\nu_{7a})_0^1$ line and overestimate the intensity of the $(\nu_{5a})_0^1$ and $(\nu_{4a})_0^1$ bands. The simulation of the intensity of the latter fundamentals is clearly one of the most demanding tasks, since the modes are involved in strong Dushinsky mixing.

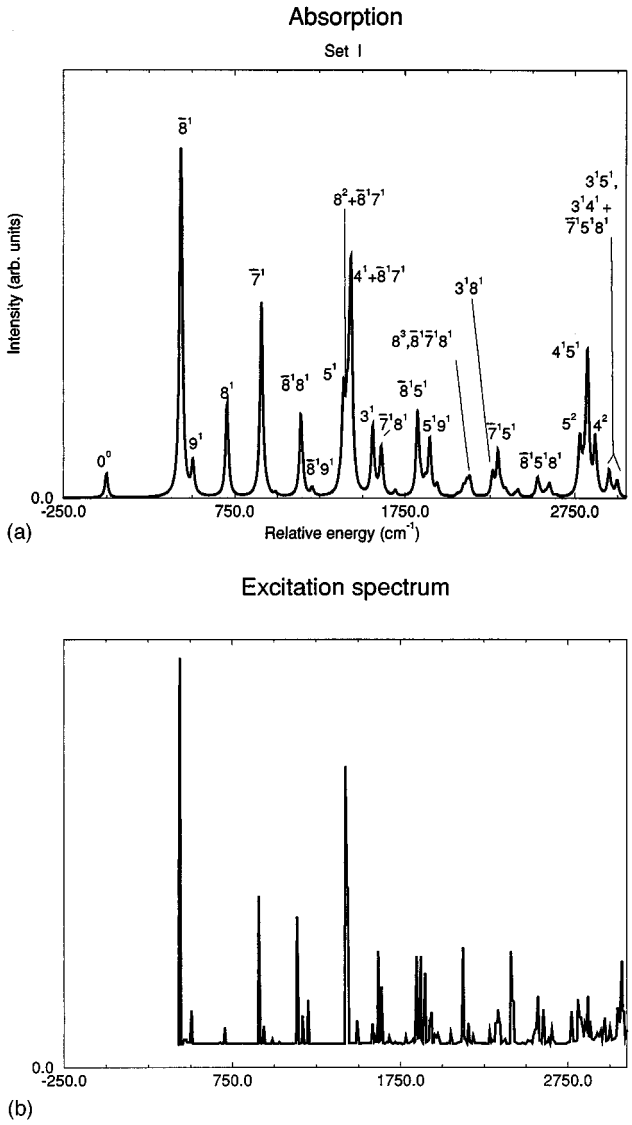

FIG. 2. Calculated absorption spectrum (a, set I) and observed (b, after Ref. 10) fluorescence excitation spectrum The linewidth used in simulation is 10 cm^{-1}.

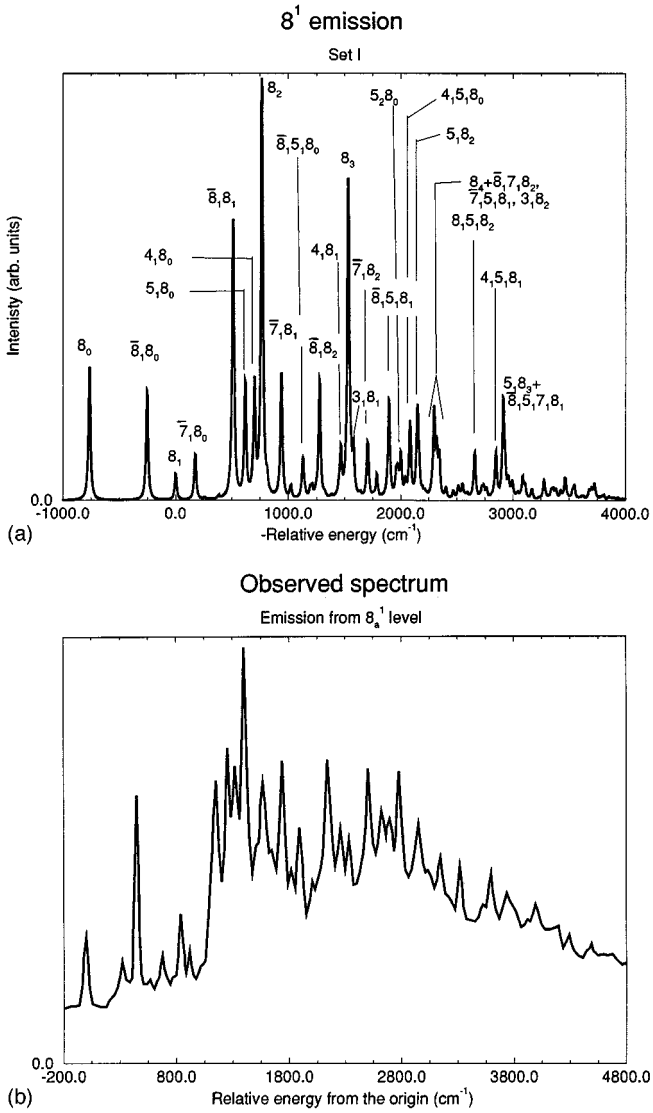

FIG. 3. Same as Fig. 1 but for the emission from the 8_a^1 level.

Moreover, the intensity of bands that include quanta of mode ν_{5a} are affected by the interference between FC and HT contributions of very similar size. The calculations also indicate that the intensity of the 1422 cm^{-1} band receives a contribution from the overtone of the ν_{8a} mode, and suggest the assignments of the 1613 cm^{-1} and 1634 cm^{-1} as the $(\nu_{3a})_0^1$ and $(\nu_{7b})_0^1(\nu_{8a})_0^1$ bands. The unassigned intense line at 1845 cm^{-1} is identified as $(\nu_{8b})_0^1(\nu_{5a})_0^1$ vibronic band.

C. SVL emission spectra from the fundamentals of the totally symmetric modes

Figures 3(a) and 3(b) show the calculated (set I) and observed (Ref. 5) $(\nu_{8a})_0^1$ SVL emission. The calculated spectrum for set II is given as Fig. 3(c) in the PAPS supplement. Set I describes the lower part of the spectrum somewhat better than set II, except for the intensity of the origin. The calculated intensity of the $(\nu_{8b})_1^0(\nu_{8a})_0^1$ band with respect to the origin of the spectrum $[(\nu_{8a})_0^1$ band] is 0.9 and 2.2 for the set I and II, respectively (experimental value given by SGK is 2.7) In agreement with the experiment the $(\nu_{8a})_2^1$ band is the most intense (3.07 and 6.05 vs 2.93). Similar values for the $(\nu_{8b})_1^0(\nu_{8a})_1^1$ band are 2.44 and 5.55 (computed) vs 2.64 (experimental). The two lines in between are identified as transitions to the fundamentals of the ν_{4a} and ν_{5a} modes. It is clear from the calculations that the $(\nu_{8a})_3^1$ band should be quite prominent in the spectrum. We think that the band assigned by SGK as $(\nu_{8b})_1^0(\nu_{7a})_1^0(\nu_{8a})_1^1$ is in fact a superposition of the overtone of ν_{8a} and the combination band. Of some interest is the reproduction of the intensity of combination bands that include quanta of the ν_{5a} mode; the medium band observed at ~1892 cm^{-1} which corresponds to the $(\nu_{8b})_1^0(\nu_{5a})_1^0(\nu_{8a})_1^1$ combination, the band at ~2000 cm^{-1} $[(\nu_{5a})_2^0(\nu_{8a})_0^1]$ and the band at ~2147 cm^{-1}

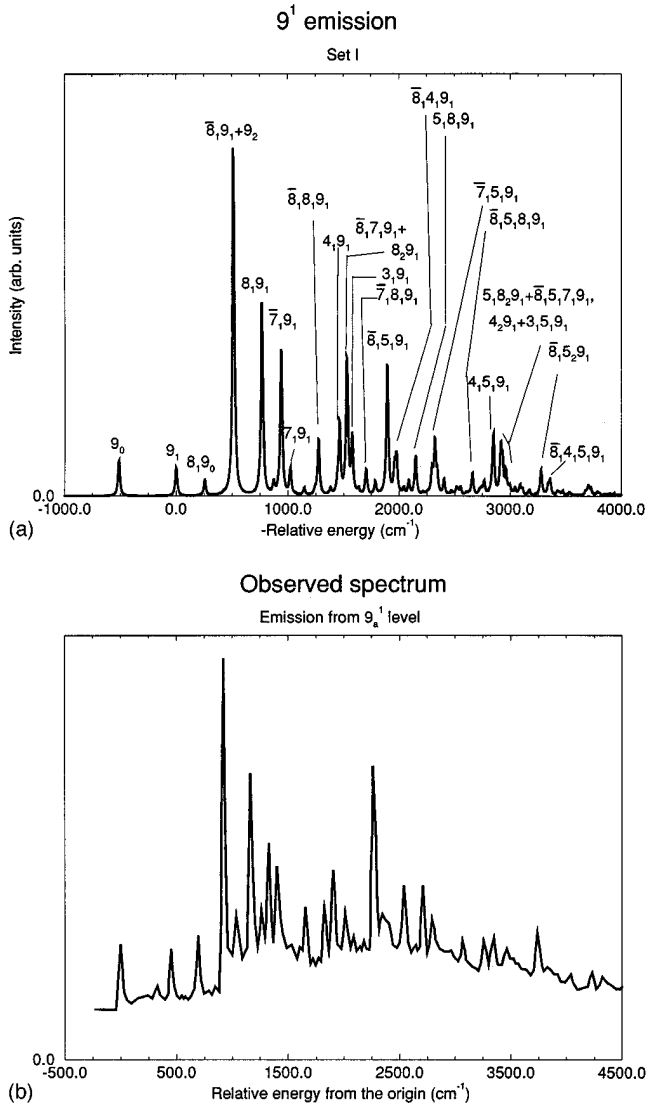

FIG. 4. Same as Fig. 1 but for the emission from the 9_a^1 level.

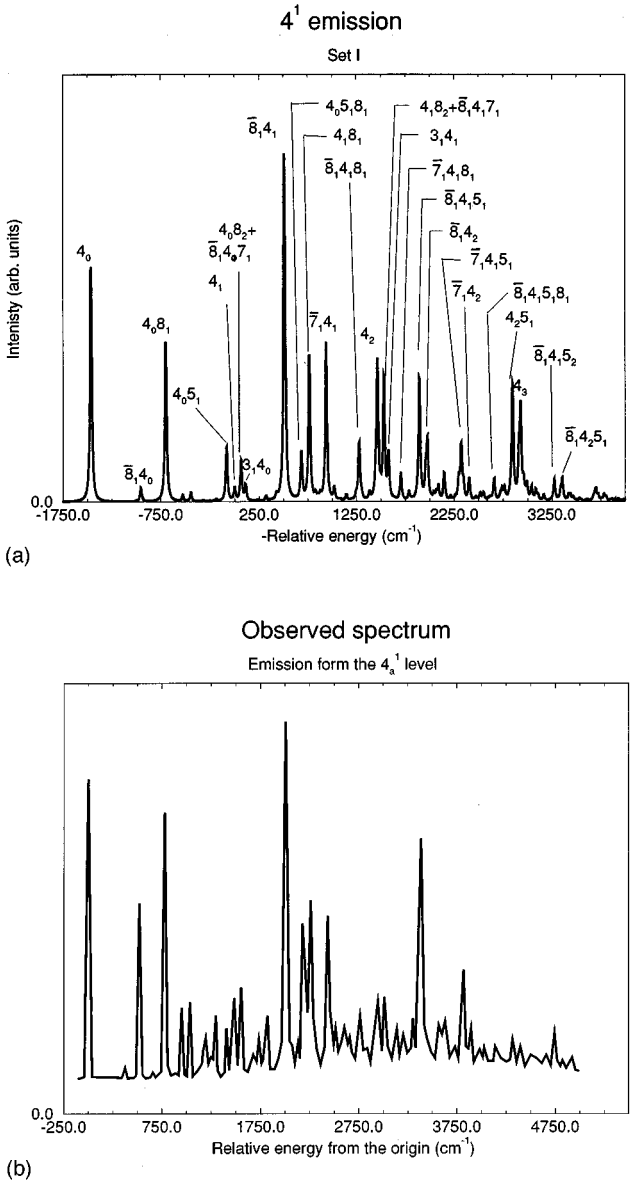

FIG. 5. Same as Fig. 1 but for the emission from the 4_a^1 level. The observed spectrum is taken from Ref. 11.

$[(\nu_{5a})_1^0(\nu_{8a})_2^1]$ are some examples of the good quality of the simulations. All other calculated bands agree reasonably well with the experimental spectrum.

Figures 4(a) and 4(b) show the calculated (set I) and observed (Ref. 5) $(\nu_{9a})_0^1$ SVL emission spectrum. The calculated spectrum for set II is given as Fig. 4(c) in the PAPS supplement. In agreement with the experiment the strongest $(\nu_{8b})_1^0(\nu_{9a})_1^1$ band is preceded by the three weak bands identified in the figures. The calculated relative intensity of the strong band with respect to the origin of the spectrum $[(\nu_{9a})_0^1$ band] is 12 and 11.3 for the set I and II vs experimentally observed value of 4.7. This intensity depends strongly on the exact value of the vibronic coupling between the S_1 and S_5 states by the ν_{9a} mode and probably on the inclusion of higher excited states in the model. This is also substantiated by a rather small calculated intensity of the $(\nu_{7a})_1^0(\nu_{9a})_1^1$ band. The band identified by SGK as the $(\nu_{8b})_1^0(\nu_{7a})_1^0(\nu_{9a})_1^1$ receives, according to our calculation, a comparable contribution also from the $(\nu_{8a})_2^0(\nu_{9a})_1^1$ band.

Figures 5(a) and 5(b) depict the calculated (set I) and observed (Ref. 11) $(\nu_{4a})^1$ SVL emission spectrum. The calculated spectrum for set II is given as Fig. 5(c) in the PAPS supplement. The quantitative reproduction of this SVL spectrum is more difficult, compared to the previous spectra, because the mode is one of the TS modes strongly involved in a Dushinsky rotation. The intensity of the origin of the spectrum is underestimated by the calculations. As it is seen it depends strongly on the details of mode mixing in the excited states. Also the intensity if the combination band $(\nu_{8b})_1^0(\nu_{4a})_0^1$ is underestimated. It is possible that the effective displacement parameter for the ν_{4a} mode is somewhat too small or that the S_1-S_5 coupling by this modes is calculated too large. However, the $(\nu_{8b})_1^0(\nu_{4a})_1^1$ band is predicted to be the strongest in the spectrum, in agreement with the experiment. Also the $(\nu_{4a})_1^1(\nu_{8a})_1^0$, $(\nu_{7b})_1^0(\nu_{4a})_1^1$, $(\nu_{4a})_2^1$ and

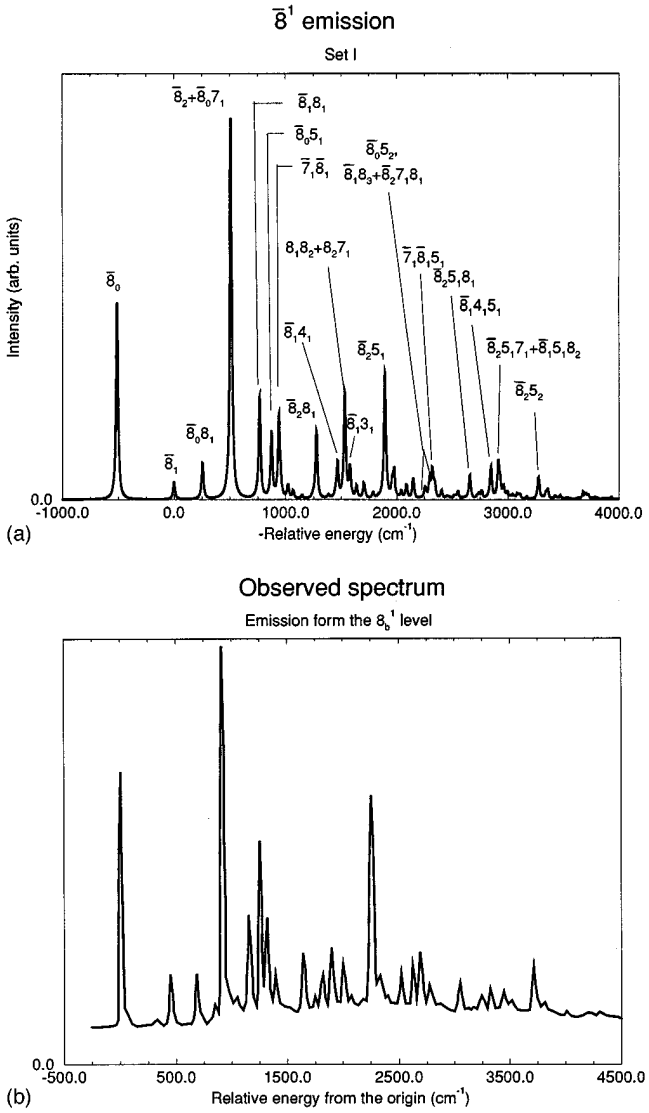

FIG. 6. Same as Fig. 1 but for the emission from the 8_b^1 level.

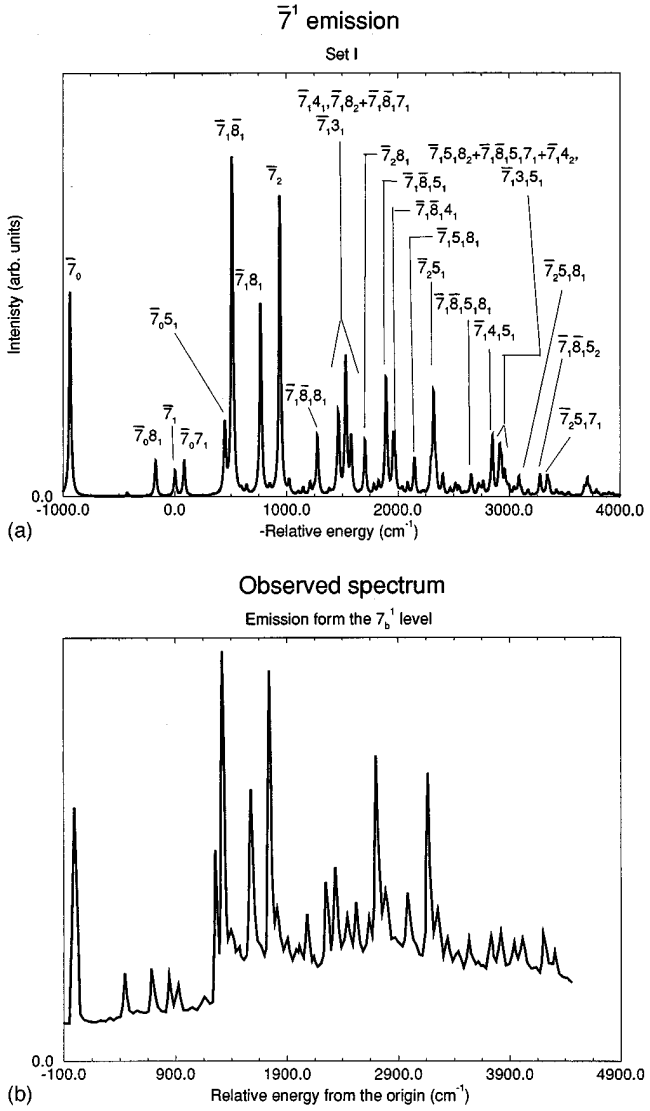

FIG. 7. Same as Fig. 1 but for the emission from the 7_b^1 level.

$(\nu_{8b})_1^0(\nu_{4a})_1^1(\nu_{5a})_1^0$ bands figure prominently in the calculated and experimental spectra.

D. SVL emission spectra from the fundamentals of the b_{3g} modes

Figures 6(a) and 6(b) show the calculated (set I) and observed (Ref. 5) $(\nu_{8b})_0^1$ SVL emission spectrum. Similar experimental spectrum was obtained by Beck *et al.* in the gas phase.[11] The calculated spectrum for set II is given as Fig. 6(c) in the PAPS supplement. The experimentally observed intensity ratio of the $(\nu_{8b})_0^1:(\nu_{8b})_1^1:(\nu_{8b})_2^1$ bands is 1:0.19:1.34 according to SGK, and 1:0.26:1.43 according to Beck *et al.*[11] The calculated ratios are 1:0.08:1.7 for set I and 1:0.17:1.7 for set II, in reasonable agreement with the experiment. The intensity ratio of the $(\nu_{8b})_0^1:(\nu_{8b})_1^1$ bands, discussed in detail in Ref. 6, is, according to SGK, 1.22. This compares very well with the calculated ratios of 1.18 and 1.21 for set I and set II of parameters. The calculations also correctly reproduce marked and almost equal intensities of the $(\nu_{8b})_1^1(\nu_{8a})_1^0$ and $(\nu_{7b})_1^0(\nu_{8b})_1^1$ bands (calculated 0.25 vs the strongest band to compare with the value of 0.26 given by SGK). The intensities of the $(\nu_{8b})_0^1(\nu_{5a})_1^0$ and $(\nu_{8b})_0^1(\nu_{5a})_2^0$ bands are, on the other hand, somewhat underestimated [calculated values of 0.20 and 0.35 vs observed 0.48 and 0.48 (Ref. 11)].

Figures 7(a) and 7(b) show the calculated (set I) and observed (Ref. 5) $(\nu_{7b})_0^1$ SVL emission spectrum. The calculated spectrum for set II is given as Fig. 7(c) in the PAPS supplement. The experimentally observed ratio of intensities of the three transitions: $(\nu_{7b})_0^1:(\nu_{7b})_1^1:(\nu_{7b})_2^1$ is 5.7:1:7.7. The calculated numbers are 8.9:1:15 for set I and 3.8:1:6 for set II. The calculated intensity of the $(\nu_{7b})_1^1(\nu_{8a})_1^0$ line is $\sim$0.8 of the intensity of the origin of the spectrum $[(\nu_{7b})_0^1]$ for both sets in perfect agreement with the experiment.

E. Emission spectra from combination bands and overtones

In this section we focus on the experimental SVL fluorescence spectrum observed after excitation to the 1422

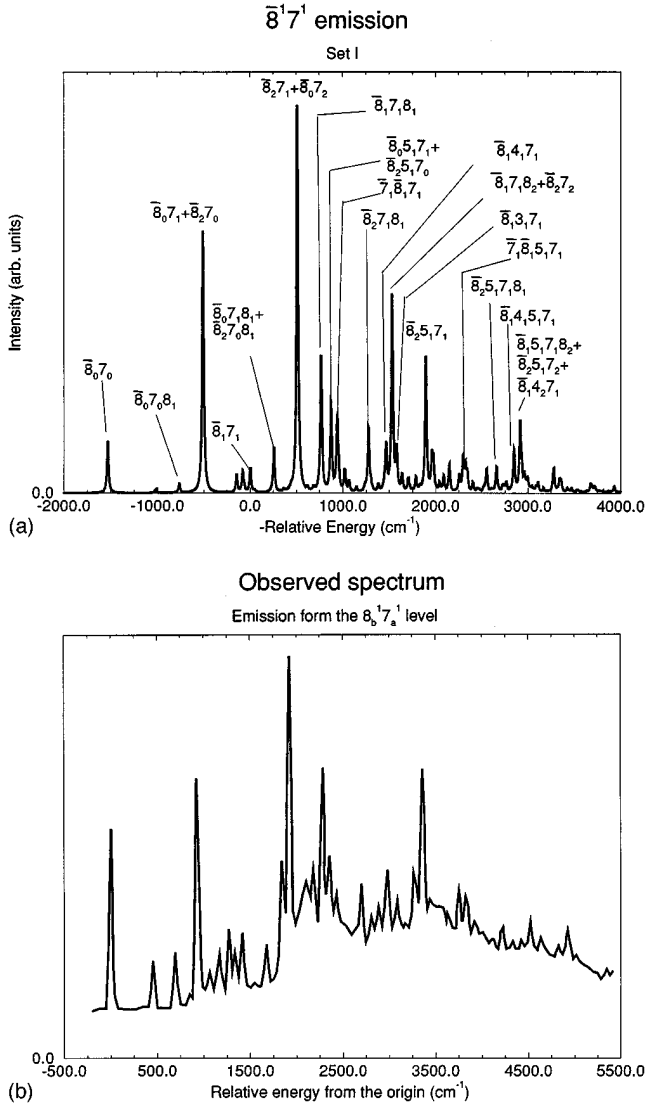

FIG. 8. Same as Fig. 1 but for the emission from the $8_b^1 7_a^1$ level.

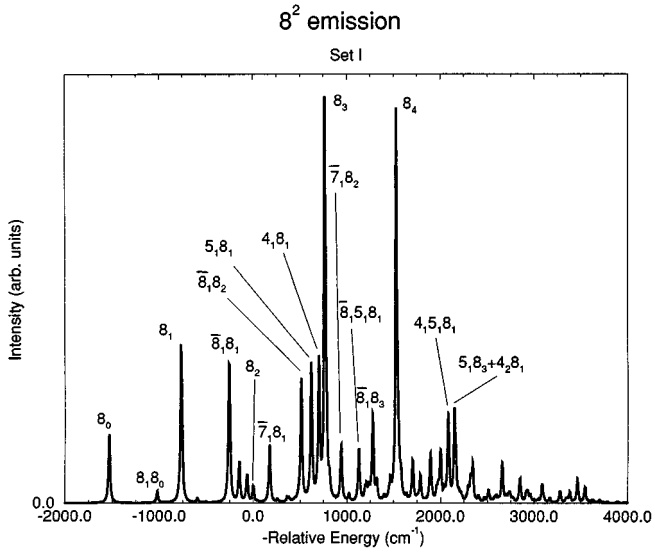

FIG. 9. Calculated (set I) emission spectrum from the 8_a^2 level. The linewidth used in simulation is 10 cm^{-1}.

cm^{-1} band (see Fig. 3 Ref. 11). The band excited in the experiment was assigned to the $(\nu_{8b})_0^1(\nu_{7a})_0^1$ level, but is is degenerate with the overtone of mode ν_{8a} and we have shown in Secs. IV A and IV B that the contribution of the overtone is predicted to be considerable.

Figure 8(a) presents the calculated spectra (set I) for the SVL emission from the $(\nu_{8b})_0^1(\nu_{7a})_0^1$ level. The calculated spectrum for set II is given as Fig. 8(c) in the PAPS supplement. The experimental spectrum after Ref. 5 is depicted in Fig. 8(b). It shows two prominent bands assigned to the $(\nu_{8b})_2^1(\nu_{7a})_0^1$ and $(\nu_{8b})_2^1(\nu_{7a})_1^1$. The observed intensity ratio of the two bands, 1:1.1, compares reasonably well with the computed 1:1.4. The simulation indicates that the two bands receive contributions also from emission to levels $(\nu_{8b})_0^1(\nu_{7a})_1^1$ and $(\nu_{8b})_0^1(\nu_{7a})_2^1$, respectively. The intensities of the origin of the spectrum $[(\nu_{8b})_0^1(\nu_{7a})_0^1]$ and of the next two bands $[(\nu_{8b})_1^1(\nu_{7a})_0^1$ and $(\nu_{8b})_0^1(\nu_{7a})_1^1(\nu_{8a})_1^0]$, are, however, underestimated by the model. The next experimentally most active mode is the ν_{5a}, which builds notable progressions on the origin and on the two main bands of the spectrum, a feature which is also reproduced by the simulation, although the intensity of the progression bands appears to be slightly underestimated. Thus, the main features of the experimental spectrum are well reproduced by the simulation of SVL fluorescence from level $(\nu_{8b})_0^1(\nu_{7a})_0^1$. Of some interest is the triplet of bands at ~1382 cm^{-1}, 1448 cm^{-1}, and 1530 cm^{-1} from the origin. Although experimentally quite weak, it is nicely reproduced by the calculation. Another relatively weak band, observed ~100 cm^{-1} to the left and assigned to the $(\nu_{8b})_0^1(\nu_{7a})_0^1(\nu_{8a})_1^0$ combination, is predicted to have negligible intensity. The underestimation of the intensity of the latter band might be due to the approximations adopted in the model. A more appealing possibility is that the intensity is due to emission from the overtone of the ν_{8a} mode which is almost degenerate with the $(\nu_{8b})_0^1(\nu_{7a})_0^1$ level.

In Fig. 9 we present the simulated spectra (set I) for the SVL emission from level $(\nu_{8a})_0^2$. The calculated spectrum for set II is given as Fig. 9(b) in the PAPS supplement. The spectrum shows the most prominent bands at 765 cm^{-1} $[(\nu_{8a})_1^2]$, 1275 cm^{-1} $[(\nu_{8a})_1^2(\nu_{8b})_1^0]$, 2295 cm^{-1} $[(\nu_{8a})_3^2]$ and 3060 cm^{-1} $[(\nu_{8a})_4^2]$ from the origin $[(\nu_{8a})_0^2]$. In addition, a number of medium intensity bands are predicted in the region 2040–2230 cm^{-1} above the origin. Most of these bands have frequencies degenerate with bands active in the spectrum of Fig. 7. As a consequence it is difficult to assess, on the basis of these bands, whether the experimental spectrum[11] results from a sum of contributions of the emission from level $(\nu_{8b})_0^1(\nu_{7a})_0^1$ (dominant) and $(\nu_{8a})_0^2$ (minor). There are, however, a few bands, namely the already mentioned $[(\nu_{8a})_1^2]$ and $[(\nu_{8a})_1^2(\nu_{8b})_1^0]$ together with the $[(\nu_{8a})_1^2(\nu_{5a})_1^0]$ and $[(\nu_{8a})_1^2(\nu_{4a})_1^0]$ which fall in regions were there is vibrational activity (experimentally) but the simulation of Fig. 7 shows negligible intensity. Thus, the results of these simulations seem to indicate that some weak

detail of the SVL fluorescence spectrum recorded by exciting the 1422 cm^{-1} level might be due to emission from the degenerate level $(\nu_{8a})_0^2$.

V. CONCLUDING REMARKS

The vibrational structure of the electronic spectra of naphthalene is simulated by using a perturbative description of the vibronic levels.

The model, which includes four excited electronic states beside the ground state, utilizes input parameters computed by quantum-chemical calculations. Transition dipole moments, structure and vibrational normal modes of the ground and excited electronic states (S_1 and S_2) are obtained from *ab initio* calculations and vibronic coupling parameters are estimated by using semiempirical methods. From the analysis of normal coordinates of the three electronic states investigated, considerable Dushinsky rotation of some of the TS modes is evidenced. The size of mode mixing in combination with the interference between FC and HT mechanisms, are the main causes of redistribution of vibronic intensities. In addition, the results of the calculations show that interference effects are very important not only for mode ν_{8a} but also for mode ν_{5a}.

The details of the vibronic structure of the spectra are reproduced, and the simulations of SVL spectra originated from NTS vibronic levels match particularly well the observed spectra. This indicates a good quality of the relative values of vibronic coupling parameters computed by semiempirical methods. The necessity to scale the computed coupling parameters by a common factor for modes of a given symmetry most probably results from the difficulty of an accurate calculation of a small (due to cancellation effects) electric dipole moment for the $S_0 \rightarrow S_1$ transition.

The simulation of the absorption spectrum indicates that the intensity of the band observed at 1422 cm^{-1} results from contributions of the $(\nu_{8a})_0^2$ overtone and $(\nu_{8b})_0^1(\nu_{7a})_0^1$ combination. On this basis it is suggested that some of the weak bands of the SVL fluorescence spectrum obtained by exciting the 1422 cm^{-1} band might be due to fluorescence from the overtone of mode ν_{8a} degenerate with the dominant emitting level $(\nu_{8b})_0^1(\nu_{7a})_0^1$.

For all the simulated spectra the intensity ratios of vibronic bands agree well with the experiment, although in some cases intensities of individual bands are overestimated or underestimated. The largest discrepancies are computed for fundamentals or combination bands of TS modes strongly involved in Dushinsky rotation, and whose intensity is determined by the interference of FC and HT mechanisms. We ascribe the discrepancies between computed and observed intensities of some of the bands, partly to the quality of the computed parameters and partly to the approximations adopted to model the spectra. Inclusion of additional electronic states and determination of geometries and mode mixing for every excited state considered in the model would improve the quantitative agreement, but is presently beyond our computational capabilities. Nevertheless the simulations provide a solid basis for a more thorough analysis of individual vibronic bands in the spectra, and are of considerable help in the assignment of doubtful bands.

ACKNOWLEDGMENT

This paper was issued as NRCC No. 39083.

[1] J. R. Platt, J. Chem. Phys. **17**, 484 (1949).
[2] W. Moffitt, J. Chem. Phys. **22**, 320 (1954).
[3] M. Gouterman, J. Mol. Spectrosc. **6**, 138 (1961).
[4] H. Sellers, P. Pulay, and J. E. Boggs, J. Am. Chem. Soc. **107**, 6487 (1985).
[5] M. Stockburger, H. Gatterman, and W. Klusman, J. Chem. Phys. **63**, 4519, 4529 (1975).
[6] M. Z. Zgierski, Chem. Phys. Lett. **47**, 599 (1977).
[7] U. Boesl, H. J. Neusser, and E. W. Schlag, Chem Phys. **15**, 167 (1976).
[8] N. Mikami and H. K. Hong, Bull. Chem. Soc. Jpn. **52**, 3484 (1979).
[9] M. Gutmann, P. F. Schönzart, and G. Hohlneicher, Chem. Phys. **140**, 107 (1990).
[10] S. M. Beck, D. E. Powers, J. B. Hopkins, and R. E. Smalley, J. Chem. Phys. **73**, 2019 (1980).
[11] S. M. Beck, J. B. Hopkins, D. E. Powers, and R. E. Smalley, J. Chem. Phys. **74**, 43 (1981).
[12] F. M. Behlen, D. B. McDonald, V. Sethuraman, and S. A. Rice, J. Chem. Phys. **75**, 5685 (1981).
[13] M. J. Robey, I. G. Ross, R. V. Southwood-Jones, and S. J. Strickler, Chem. Phys. **23**, 207 (1977).
[14] A. Warshel and M. Karplus, J. Am. Chem. Soc. **94**, 5612 (1972).
[15] F. Zerbetto, M. Z. Zgierski, F. Negri, and G. Orlandi, J. Chem. Phys. **89**, 3681 (1988).
[16] J. Del Bene and H. H. Jaffe, J. Chem. Phys. **48**, 1807 (1968).
[17] GAUSSIAN 92/DFT, Revision G.2, M. J. Frisch, G. W. Trucks, H. B. Schlegel, P. M. W. Gill, B. G. Johnson, M. W. Wong, J. B. Foresman, M. A. Robb, M. Head-Gordon, E. S. Replogle, R. Gomperts, J. L. Andres, K. Raghavachari, J. S. Binkley, C. Gonzalez, R. L. Martin, D. J. Fox, D. J. Defrees, J. Baker, J. J. P. Stewart, and J. A. Pople Gaussian, Inc., Pittsburgh, Pennsylvania, 1993.
[18] M. Z. Zgierski, J. Chem. Phys. **85**, 109 (1986).
[19] P. Swiderek, G. Hohlneicher, S. A. Maluendes, and M. Dupuis, J. Chem. Phys. **98**, 974 (1993).
[20] P. Pulay, G. Fogarasi, and J. E. Boggs, J. Chem. Phys. **74**, 3999 (1981).
[21] J. B. Foresman, M. Head-Gordon, J. A. Pople, and M. J. Frisch, J. Chem. Phys. **96**, 135 (1992).
[22] G. Orlandi, P. Palmieri, R. Tarroni, F. Zerbetto, and M. Z. Zgierski, J. Chem. Phys. **100**, 2458 (1994).
[23] M. Z. Zgierski and F. Zerbetto, J. Chem. Phys. **99**, 3721 (1993).
[24] M. Z. Zgierski and F. Zerbetto, J. Chem. Phys. **98**, 14 (1993).
[25] F. Zerbetto and M. Z. Zgierski, J. Chem. Phys. **98**, 4822 (1993); **101**, 1842 (1994).
[26] L. M. Markham, L. C. Mayne, B. S. Hudson, and M. Z. Zgierski, J. Phys. Chem. **97**, 10 319 (1993).
[27] F. Negri and M. Z. Zgierski, J. Chem. Phys. **100**, 2571 (1994).
[28] F. Negri and M. Z. Zgierski, J. Chem. Phys. **99**, 4318 (1993).
[29] F. Negri and M. Z. Zgierski, J. Chem. Phys. **102**, 5165 (1995).
[30] G. Orlandi, Chem. Phys. Lett. **44**, 277 (1976).
[31] C. P. Brock and J. D. Dunitz, Acta Crystallogr. B **38**, 2218 (1982).
[32] K. K. Innes, in *Excited States*, edited by E. Lim (Academic, New York, 1975), Vol. 2.
[33] J. M. O. Matos and B. O. Roos, Theor. Chim. Acta **74**, 363 (1988).
[34] G. Hohlneicher and J. Wolf, Ber. Bunsenges. Phys. Chem. **99**, 366 (1995).
[35] F. Dushinsky, Acta Phisicochim. USSR **7**, 551 (1937).
[36] C. Manneback, Phys. Utrecht **17**, 1001 (1951).
[37] E. B. Wilson, J. C. Decius, and P. C. Cross, *Molecular Vibrations* (McGraw–Hill, New York, 1955), p. 290.
[38] See AIP document No. PAPS JCPSA6-104-3486-9 for 9 pages of figures. Order by PAPS number and journal reference from American Institute of Physics, Physics Auxiliary Publication Service, Carolyn Gehlbach, 500 Sunnyside Boulevard, Woodbury, NY 11797-2999. Fax: 516-576-2223, e-mail: janis@aip.org. The price is $1.50 for each microfiche (98 pages) or $5.00 for photocopies of up to 30 pages, and $0.15 for each additional page over 30 pages. Airmail additional. Make checks payable to the American Institute of Physics.